Design and Analysis of A Pico Propeller Hydro Turbine Applied in Fish Farms using CFD and Experimental Method

Bao Ngoc Tran[*] · Jun-ho Kim[**†]

* Graduate School of Mokpo National Maritime University, Mokpo 58628, Korea
** Division of Marine Mechatronics, Mokpo National Maritime University, Mokpo 58628, Korea

Abstract : *In this paper, a pico hydro turbine employing low head circulation water at fish farms is designed and evaluated. Due to the advantages of simple structures, small head requirements, and low-cost investment, the constant thickness propeller turbine is considered as a feasible solution. The design process based on the free vortex method is presented in full detail, and a 4-blade runner is built using BladeGen. The turbine performance is analyzed both numerically and via experimental methods. Despite slight differences, the results show similar trends between CFD simulations and experiments carried out on factory test-rigs in a wide range of working conditions. At the design flow rate, the turbine achieves the best efficiency of 70 %, generating 3.5 kW power when rotating at 420 rpm. The internal flow field, as well as the turbine's behavior, are investigated through the distribution of blade streamlines, pressure, and velocity around the runner. Moreover, the pressure coefficient on the blade surface at 3 span positions is plotted while the head loss for each simulation domain is calculated and displayed by charts.*

Key Words : *CFD, Propeller hydro turbine, Low head, Fish farms, Performance*

1. Introduction

In our fast-changing world, renewable energy increasingly plays an essential role in every industrial field. Among several types of renewable energy, hydro energy stands as the most commonly used source with a vast amount of power scales and applications. A record 4185 TWh in electricity was generated from hydropower in 2017, avoiding production of approximately 4 billion tons of greenhouse gases and harmful pollutants.

Small scale hydropower plants with the output below 5 kW are classified as pico-hydropower plants. Despite the fact that pico turbines possess a number of advantages, including low-cost investment, simple structure, and high flexibility, this type of hydro turbine still receives less attention from researchers and engineers. A model of propeller turbine with a spiral casing, developed by Simpson (Simpson and Williams, 2011), achieved an overall efficiency of 65 % with a field-installed turbine. Several researchers applied a combination of experiment and CFD approaches for turbine investigation (Lee et al., 2012; Vu et al., 2018), in which a counter-rotating tubular turbine and a pipeline-installed turbine were analyzed. Axial-flow turbines for low head micro hydro systems (between 4 m to 9 m) were introduced by Alexander

(Alexander et al., 2009). Hydraulic efficiency of over 68 % was achieved in all test models, which were built using planar blades. Samora carried out research to figure out the characteristics of the 5-blade propeller turbine used for water supply and distribution networks (Samora et al., 2016). The experimental analysis proved that this turbine reached an efficiency of around 60 % with a flow rate from 15 to 20 m³/h. An improvement of 19 % in hydraulic efficiency was gained by altering the inlet and exit tip angle of a propeller runner blade which was designed based on free vortex methods in an experimental optimization conducted by Singh (Singh and Netmann, 2009). After three stages of blade geometry modification, the final runner configuration performed at a maximum efficiency of 74 % under a gross head of 1.75 m.

Most of the recent studies have paid concentration on the large scale power systems which are not appropriate for low-head and low-flow applications. A few research involved in pico turbines but the required head (from 4 m to 20 m) still is a barrier. In this paper, the design process and performance of a pico propeller hydro turbine working at very low head sites are presented. This pico turbine is not only capable of operating with a head of 2 m, but also possesses a simple profile runner, facilitating the manufacturing work. The turbine is employed at the fish farms where the low head circulation water is available all year round. With a low-cost investment, it harnesses the hydropower of

* First Author : ngoctranbao.hn@gmail.com, 061-240-7472
† Corresponding Author : junho.kim@mmu.ac.kr, 061-240-7241

circulation water to supply electricity for local demands. The turbine prototype was made and then its performance was tested numerically and experimentally. The output power, as well as hydraulic efficiency, are measured and compared. Besides, computational simulations contribute to investigate the internal flow field and predict turbine's characteristics.

2. Turbine Design Methodology

Due to the goal of designing an effective hydro turbine possessing a simple structure, a propeller turbine with constant thickness runner blades is chosen as the target model to carry out the research. Based on the free vortex theory, the runner design procedure contains a series of logical calculations steps. Several researchers employed this well-known method to develop their own turbine runner blades (Singh et al., 2009; Muis and Sutikno, 2014). Dixon (Dixon, 2004) claimed that the free vortex theory is applicable not only to incompressible flow for hydraulic turbines, but also the compressible flow for axial compressor and gas turbines. Since the propeller turbine belongs to the axial flow type, it is sensible to apply the free vortex theory in designing this turbine.

The flow chart in Fig. 1 outlines the stages of the runner design process. To facilitate the manufacture, shape and dimensions of the runner it may be required to adjust through a number of iterations with the purpose of avoiding the large twist blade or reverse angle at the hub inlet. The design starts with the selection of the turbine's key parameters, including rated flow rate (Q), gross head (H), and rotational speed (N). After checking the specific speed (N_s) to ensure that N_s is in the range fitted for the propeller turbine, calculations of tip and hub diameter are conducted. These aforementioned parameters are determined by the following equations:

$$N_s = \frac{N\sqrt{P}}{H^{5/4}} \tag{1}$$

$$D_t = \frac{60.k_{ug}.\sqrt{2gH}}{\pi N} \tag{2}$$

$$v_a = \frac{Q}{A} = \frac{4Q}{\pi(D_t^2 - D_h^2)} \tag{3}$$

where N_s is the specific speed, P is the output power, D_t and D_h are the blade tip and hub diameter, k_{ug} is the ratio of tip velocity to head velocity.
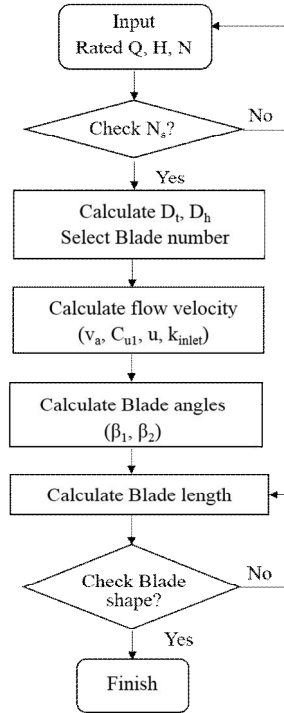

Fig. 1. Runner design flow chart.

In the next step, the axial and tangential velocities for each blade section are specified. The axial flow through the runner, which is invariable over the sections, is calculated using Equation 3. According to the law of angular momentum conservation, the free vortex principle can be illustrated via Equation 4. Applying this condition to each blade section, the product of tangential velocity and section radius must be constant at both the blade inlet and exit (presented by Equation 5).

$$C_u.r = k \tag{4}$$

$$C_{u1}.r = k_{inlet} \quad \text{and} \quad C_{u2}.r = k_{exit} \tag{5}$$

where C_{u1}, C_{u2} are tangential velocities at inlet and exit, k is a constant for free vortex flow, r is the section radius.

Constant k is a key point for determining the value of flow tangential velocities. Generally, the constant k at the inlet is involved in Euler's head equation and can be calculated with:

$$k = \frac{\eta gH}{2\pi.\dfrac{N}{60}} \tag{6}$$

In order to mitigate any loss caused by swirl flow and maximize the energy absorbed from fluid, it is assumed that there

is no whirl located at the exit region. Therefore, $C_{u2} = 0$ and the constant $k_{exit} = 0$ all along the exit profile of the runner blade.

The inlet and exit velocity triangles at each blade section are illustrated in Fig. 2. The runner blade in the current study is equally divided into seven sections from hub to tip. The inlet and exit flow angles at a certain section are determined by the below expressions:

For inlet position: $\alpha_1 = tan^{-1}(\dfrac{v_a}{u - C_{u1}})$ (7)

For inlet position: $\alpha_2 = tan^{-1}(\dfrac{v_a}{u})$ (8)

where u is the blade tangential velocity ($u = r\omega$).

Hence, the inclined angle of the blade at the leading edge (β_1) and trailing edge (β_2) are also calculated. Because of the rise of tangential velocity u and the reduction of C_{u1} component from hub to tip, the flow angle (α_1, α_2) and blade angle (β_1, β_2) also change as a result. The details of the relative flow angle along the runner blade are displayed in Table 1.

The turbine is developed for a gross head of 2 m, a rated flow of 0.25 m³/s, and a rotational speed of 450 rpm. An 80 % hydraulic efficiency is assumed, and a hub-to-tip ratio (D_h/D_t) of 0.4 is taken into consideration. The turbine runner consists of 4 blades and the pitch to chord ratio ranges between 0.7 and 0.9 (from hub to tip). The selections of hub-to-tip ratio, as well as the blade number, are based on the turbine specific speed N_s, according to the recommendation of Simpson (Simpson and Williams, 2011). Alexander (Alexander et al., 2009) designed a propeller turbine with D_h/D_t greater than 0.6 while Vu (Vu et al., 2018) chose 0.5 as a preferred ratio. After calculations for determining the blade parameters were conducted, the 3D geometry of the runner is created in BladeGen Module - a component of ANSYS BladeModeler. This software provides users easy-to-use tools for the rapid 3D design of rotating machinery components and can be used to design a series of machinery such as pumps, compressors, fans, turbines, turbo-chargers, and inducers. The design parameters of the turbine are summarized in Table 2, and a 3D model of the turbine runner is shown in Fig. 3.
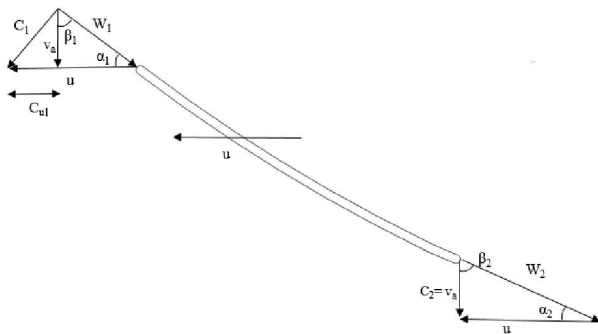

Fig. 2. Inlet and exit velocity triangles.

Table 1. Inlet and exit blade angles

Diameter ratio (d/Dt)	Inlet blade angle (β_1)	Exit blade angle (β_2)
0.4	20	55
0.5	29	60
0.6	46	64
0.7	57	67
0.8	63	70
0.9	67	72
1	70	73

Table 2. Turbine design parameters

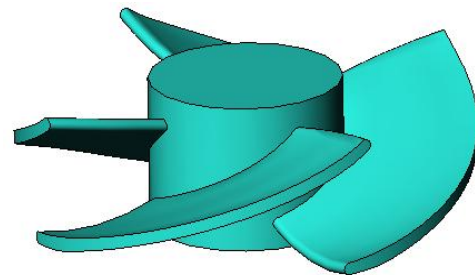| Parameters	Signal	Unit	Value
Power Output	P	kW	3
Expected Efficiency	η	-	0.8
Gross Head	H	m	2
Flow rate	Q	m³/s	0.25
Rotational speed	N	RPM	450
Tip diameter	D_t	m	0.38
Hub-to-tip ratio	D_h/D_t	-	0.4
Number of Blade	Z	-	4

Fig. 3. Runner blade geometry.

3. Experimental and numerical method

3.1 Experimental test-rig

The experimental test-rig was installed and tested by Daea Company, Samho Industrial zone, Mokpo, Korea. The outline of the experimental test-rig detailed sizes is presented in Fig. 4 and the equipment is displayed in Fig. 5. The apparatus consists of a water basin, a water tank, a permanent magnet generator, a vertically installed propeller turbine, three supplied pumps, and an ultrasonic flow meter (AquaTrans AT600). In addition, pipeline and gate valves are also equipped. The inner diameter of the pipes is 384 mm whereas the tip diameter of the runner is 380 mm, so the tip clearance between the blade tip and inner pipe wall of 2 mm is implemented. Water in the basin is supplied to the upper tank by means of the feed pumps. In order to ensure the gross head requirement, the tank is positioned 2 m higher than the turbine installation position. Depending on the required flow rate, one, two, or three pumps can be operated simultaneously. During the operation of the turbine, the speed is recorded by means of a hand digital tachometer (DT-2334C Model). Meanwhile, the output power generated by the generator is collected and measured with a SKY-500 inverter. All measurement signals of equipment are recorded by a data logger, and this datum is then calculated and compared with the numerical prediction results.

To characterize the performance of the turbine, the experiment is conducted in the test-rig, covering a range of flow rate from 0.22 m^3/s to 0.3 m^3/s. The flow rate varies by means of combining the usage of feed pumps and gate valves. The fixed excitation of the magnet generator increase the difficulty of keeping the generator (also the turbine) rotational speed constant at all load points. Therefore, at each value of the flow rate, the turbine rotates at a certain speed while the gross head is unchanged. All parameters including flow rate, speed, voltage, and current are measured and recorded. Based on the measurement results, detailed calculations are performed in order to plot the efficiency curve and power curve at a number of working points.

3.2 Numerical method
3.2.1 Turbulence model

Along with the experiment, the numerical analysis, using a commercial CFD code - CFX was also carried out to predict the turbine performance, as well as to investigate the flow field of the fluid through the runner. This multi-purpose code is capable of solving the three dimensional Reynolds Average Navier-Stock
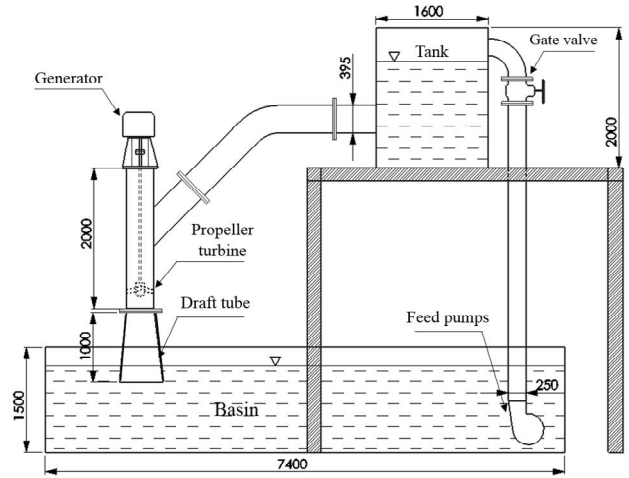

Fig. 4. Test-rig outline.

(a) Turbine installation   (b) Generator

(c) Feed pumps   (d) Inverter

Fig. 5. Experimental apparatus.

(RANS) equation for steady and turbulent fluid flow, especially in the field of turbo-machinery simulations and analyses.

The turbulence model is an important factor in deciding the

accuracy of the simulations. As referenced in several documents, the SST (Shear Stress Transport) turbulence model takes the advantages of the combination of k-ε in the far field and k-ω in the viscous sub-layer at the near wall regions. The validation of the SST turbulence model can be found in research on hydraulic turbine performance done by Muis (Muis and Sutikno, 2014), Byeon (Byeon and Kim, 2013), and Chen (Chen et al., 2014). It is found that SST shows is capable of estimating the vortex appearance and flow separation on the surfaces of complex geometry blades. With the aforementioned merits, SST turbulence model is employed in the numerical analysis of the current study.

3.2.2 Mesh formation and boundary conditions

The grid of fluid domains are generated with the Turbo-Grid module in ANSYS Workbench, based on structured hexahedra elements which are space efficient, and provide the simulations a better convergence and a higher resolution. The three main components, including suction domain, runner domain, and draft tube domain, are all built and meshed simultaneously. The refined mesh is implemented at the blades' hub and shroud to achieve a higher mesh density and an inflation of 10 layers is applied to all wall surfaces for increasing the accuracy of calculations of the flow field at near wall regions. Fig. 6 displays the mesh formation of the runner blade while Table 3 contains the Y-plus value and mesh information for each domain.
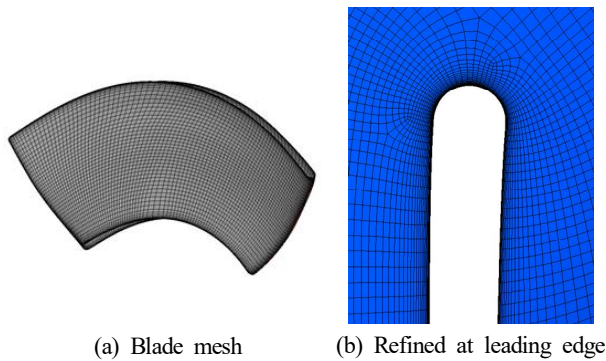

(a) Blade mesh   (b) Refined at leading edge

Fig. 6. Runner blade mesh formation.

Table 3. Mesh parameters (a quarter of full geometry)

Domains	Average Y+	No. of Elements
Suction	0.61	142,000
Runner	5.13	459,600
Draft tube	0.85	292,000
Total	-	893,600

For saving computational resource and calculation time, one-fourth domain simulations are conducted, applying periodic interfaces to each fluid domain. The boundary conditions for simulations are given in Table 4. At the inlet of the suction domain, a total pressure is set corresponding to a gross head of 2 m. Meanwhile, the outlet applies various values of mass flow rate to characterize the turbine performance under different working conditions. Water at 25°C is chosen as the working fluid, and the convergence criterion of the simulations is 10^{-5}.

Table 4. Boundary conditions

Conditions	Value
Analysis type	Steady state
Turbulence model	SST
Rotor-Stator Interface	Frozen rotor
Inlet	Total pressure
Outlet	Mass flow rate
Convergence criterion	10^{-5}
Wall	Smooth, No-slip

4. Results and discussion

During the turbine performance's test, a series of working conditions are implemented. The turbine firstly runs at the low flow, then the flow rate increases step by step by putting more feed pumps into operation. Measurement data at every operating point is recorded. Numerical simulations are also taken placed under the same conditions so as to compare and validate the results. The hydraulic power, output power, and hydraulic efficiency are calculated using the following equations:

$$P_h = \eta_h \rho g Q H \tag{9}$$

$$P_{mec} = T.\omega \tag{10}$$

$$P_{output} = U.I \tag{11}$$

$$\eta_h = \frac{P_{mec}}{P_h} \tag{12}$$

where P is the power (W), ρ is water density (kg/m³), η_h is the expected efficiency, Q is the flow rate (m³/s), H is the gross head (m), T is the torque on runner blade (N.m), ω is the rotational speed (rad/s), I is the current intensity (A), U is the voltage (V).
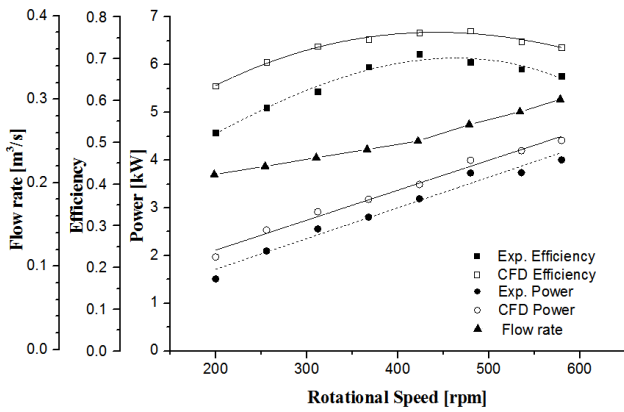
Fig. 7. Performance curves of the propeller turbine.

Fig. 7 shows the relationships of the hydraulic efficiency and power to the rotational speed for both numerical and experimental methods. Two characteristics are investigated over a wide range of speeds, from 200 rpm to 580 rpm. In general, the output power and efficiency of the simulation data follow the same trend as that found in the experimental results. As for the efficiency curve, the most significant feature is that as rotational speed rises, the efficiency increases gradually, tops near the design point and then drops following excess rotation. The maximum efficiency for the numerical simulation and experiment were 0.76 and 0.7 in turn, peaking at a rotational speed of 420 rpm. As can be seen, the gap between the two methods is larger at lower speeds and shrinks at the best efficiency point (BEP). Meanwhile, the output power progressively increase over the range of speed. A higher flow rate induces faster rotation of the runner, resulting in higher power generation. The smallest gap between the numerical and experimental power output can be observed at a speed of 420 rpm, being 9 %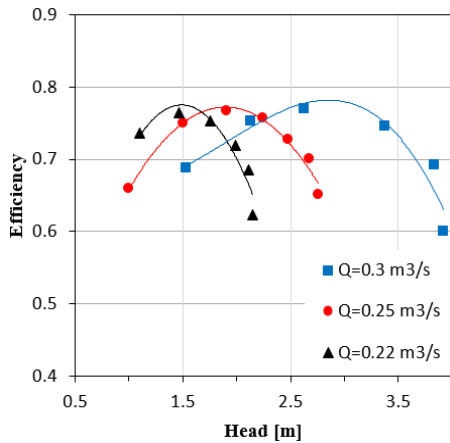. Reasons for the above disparities are other types of head loss in actual operating condition as well as the measurement error of testing equipment. In the simulations, volumetric loss at the tip clearance, friction loss at the component's surfaces, and mechanical loss at the bearing and shaft are needed to be included in turbine performance prediction. In this way we can further reduce the difference between simulation and experimental results.

The relationship between efficiency and head at three values of flow rate including 0.22 m³/s, 0.25 m³/s, and 0.3 m³/s is displayed in Fig. 8. For each flow rate case, the change in rotational speed leads to the variation of the effective head, which is determined by Equation 13.

$$H = \frac{P_{inlet} - P_{outlet}}{g\rho} \tag{13}$$

where H is the effective head (m), P_{inlet} and P_{outlet} are the average pressure at the inlet and outlet of the fluid domain (Pa).

For each flow rate, the turbine operates effectively at a different range of head, although the maximum efficiency remains 75-76 % in any case. At excess flow rate, the head corresponding to BEP is 3 m. While at the designed flow of 0.25 m³/s, the turbine performs best around a head of 2 m which is fitted for low head applications at fish farms. Fig. 9 illustrates the distribution of the streamline on the blade surface with different cases of rotational speed. It is obvious that the streamline at rated speed is the

Pressure side   Suction side

(a) Case 1: 250 rpm

(b) Case 2: 450 rpm

(c) Case 3: 550 rpm

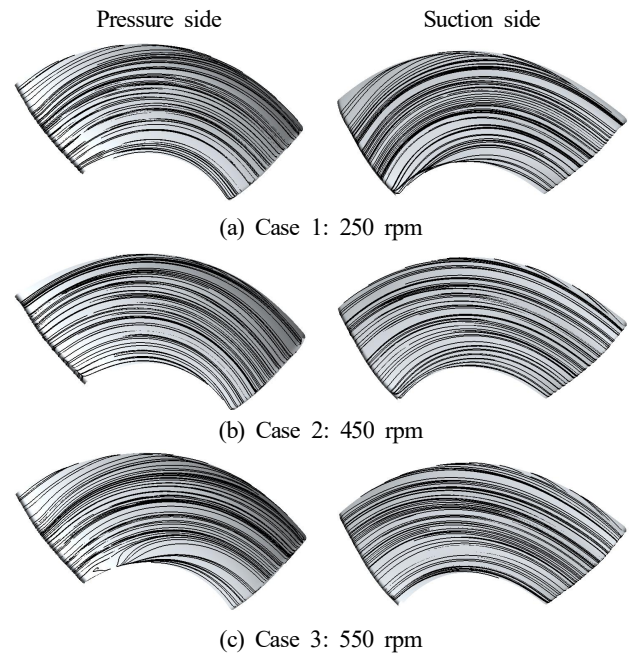Fig. 8. Efficiency versus head at different flow rate.

Fig. 9. Streamline on the runner surface.

smoothest and most evenly distributed. Whereas, the suction side of case 1 and the pressure side of case 3 experience a slight flow separation at the blade leading edge. The negligible secondary flow at partial and excess speed brings out that the runner is well designed to operate under a wide range of rotations without significant impact on hydraulic performance.

Concerning the internal flow, Fig. 10 shows the pressure contour and velocity vectors within the simulation domain at the design point. In terms of the pressure distribution, after passing through the runner the fluid pressure suddenly drops from 20 kPa to 4 kPa, indicating that the majority of fluid energy is converted to the kinetic energy of the runner, and then is transformed into electricity by means of the magnet generator. The relatively high efficiency at design condition (Fig. 8) contributes to prove the turbine's effective energy absorbability. Turning to the velocity vectors, there is a low-velocity region at the draft tube center right behind the turbine's hub. In this area, the reverse flow is likely to appear which should be suppressed to improve the turbine performance.

Pressure coefficient, which is calculated by Equation 14, is a reliable factor to evaluate the turbine behavior.

$$C_p = \frac{P_{local} - P_{aver}}{\rho g H} \tag{14}$$

$$H_{loss} = \frac{\Delta P}{\rho g H} \tag{15}$$

$$H_{loss-Runner} = \frac{\Delta P_R - T.\omega/Q}{\rho g H} \tag{16}$$

where C_p is the pressure coefficient, P_{local} and P_{aver} are the local and average static pressure on the blade surface (Pa), ΔP_R is the total pressure reduction in runner domain (Pa).

Fig. 11 demonstrates the variation of pressure coefficient at 3 span locations namely r/R = 0.1, 0.5, and 0.9 along the stream-wise direction. The pressure discrepancy between the pressure side and suction side of the blade causes the thrust force and torque which make the runner rotate. Hence, the greater the pressure discrepancy is, the higher the torque is generated. As can be seen, on the pressure side, the pressure coefficient at span 0.9 is the highest, followed by span 0.5 and span 0.1 is the lowest. In all spans, the pressure disparity is located mainly at the leading edge and middle of the blade from 0.1 to 0.8 stream-wise direction while the trailing edge witnesses a minor pressure difference.

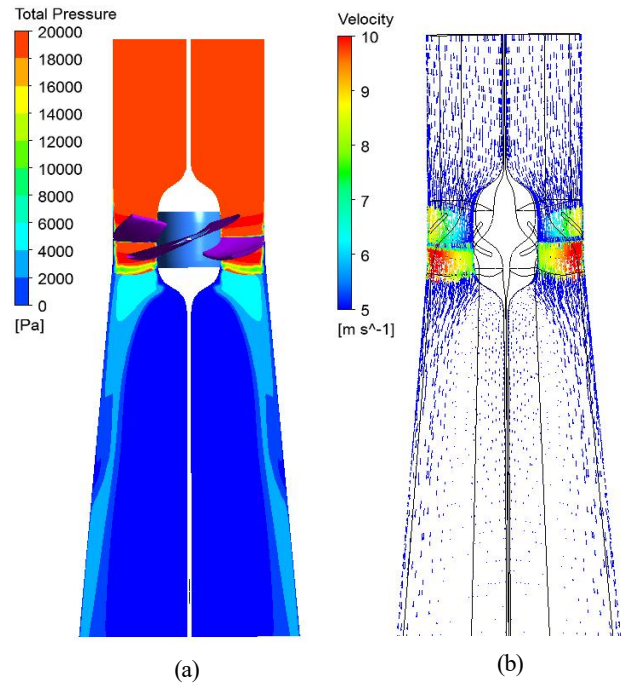(a)   (b)
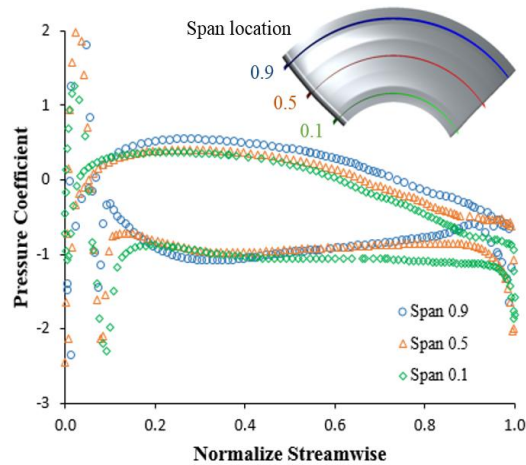
Fig. 10. Pressure contour and velocity vectors.

Fig. 11. Pressure coefficients at 3 cross sections.

Investigation in the head loss for each of the calculation domains is conducted using the results collected by numerical simulations. Head loss was discovered in three fluid regions including the intake domain, runner domain, and draft tube domain. Equations 15 and 16 are employed in order to calculate the head loss for each area.

Fig. 12 shows the comparison between the head loss for each domain in the 4 cases of rotational speed while the flow rate remains at Q=0.25 m^3/s. It is clearly seen that the total loss at speed of 450 rpm is the smallest and loss at the intake domain is

Bao Ngoc Tran · Jun-ho Kim

negligible for all cases. The intensity of head loss in runner and draft tube witness an opposite trend. With the rise of rotational speed, the draft tube loss decreases while runner loss increases gradually, rocketing to 22 % in excess rotation. The total head loss of all domains is in inverse proportion to the turbine hydraulic efficiency.
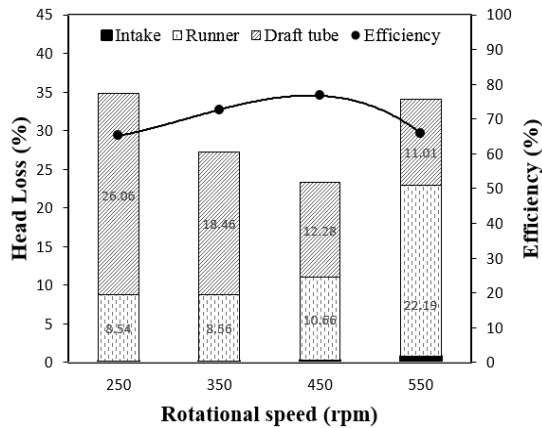

Fig. 12. Head loss of each component at design flow rate.

5. Conclusion

This paper presents the design process along with numerical and experimental studies on the performance of a pico propeller hydro turbine. The simulations and experiments are conducted under various working conditions to derive some key points as following:

The propeller turbine designed based on the free vortex method operates in a wide range of flow rate and rotational speeds, achieving maximum efficiency of 76 % and 70 % in numerical and experimental results, respectively. At the design condition, an output power of 3580W is generated. The CFD prediction for turbine performance is validated via experimental testing, displaying a relatively good agreement.

The smooth streamline reveals effective operation of the runner with minor separation flow. Calculated head loss proves a close tie between the turbine efficiency and the total head loss.

The simple structure of the propeller turbine not only facilitates the manufacturing work but also its applications. The turbine is firstly developed for harnessing circulation water used in fish farms but it can be widely employed for a number of low head sites, especially in remote mountainous areas.

References

[1] Simpson, R. and A. Williams(2011), Design of propeller turbines for pico hydro, Available at www.picohydro.org.uk.

[2] Lee, N. J., J. W. Choi, Y. H. Hwang and Y. H. Lee(2012), Performance analysis of a counter-rotating tubular type micro-turbine by experiment and CFD, 26th IAHR Sym, Hydraulic Machinery & Systems Proceeding, pp. 1-8.

[3] Alexander, K. V., E. P. Giddens, and A. M. Fuller(2009), Axial-flow turbines for low head microhydro systems, Renewable Energy, Vol. 34, No. 1, pp. 35-47.

[4] Samora, I., V. Hasmatuchi, C. M. Alligne and M. J. Fanca(2016), Experimental characterization of a five blade tubular propeller turbine for pip inline installation, Renewable Energy, Vol. 95, pp. 356-366.

[5] Singh, P. and F. Nestmann(2009), Experimental optimization of a free vortex propeller runner for micro hydro application, Exp. Thermal and Fluid Science, Vol. 33, No. 6, pp. 991-1002.

[6] Muis, A. and P. Sutikno(2014), Design and simulation of very low head axial hydraulic turbine with variation of swirl velocity criterion, Int. J. Fuild Machinery and System, Vol. 7, No. 2, pp. 68-79.

[7] Dixon, S. L.(2004), Fluid Mechanics Thermodynamics of Turbo Machinery-5th Edition, Elsevier B. Heinemann.

[8] Vu, V. L., Z. Chen and Y. D. Choi(2018), Design and performance of a pico propeller hydro turbine model, J. Fluid Machinery, Vol. 21, No. 3, pp. 44-51.

[9] Byeon, S. S. and Y. J. Kim(2013), Influence of Blade Number on the Flow Characteristics in the Vertical Axis Propeller Turbine, Int. J. Fuid Machinery and Systems, Vol. 6, No. 3, pp. 144-150.

[10] Chen, Z., J. C. Kim, M. H. Im, and Y. D. Choi(2014), Analysis on the performance and internal flow of a tubular type hydro turbine for vessel cooling system. J. Korean Society of Marine Engineering. Vol. 38, No. 10, pp. 1244-1250.